Complex band structure, decay lengths, and Fermi level alignment in simple molecular electronic systems

John K. Tomfohr and Otto F. Sankey
Department of Physics and Astronomy, Arizona State University, Tempe, Arizona 85287
(Received 10 December 2001; published 28 May 2002)

The complex band structure of a periodic system is the conventional band structure extended to complex Bloch k vectors. The k vectors with an imaginary part describe spatially decaying wave functions and arise in, for example, the analysis of impurity and surface states. They also represent the quantum tunneling states which are vehicles of electron transport through a barrier such as a thin oxide layer or a molecule. We present a method for obtaining the complex band structure of a molecule which is composed of repeating units. The complex band structures of some simple organic molecules (n-alkanes, alkenes, and linked benzene rings) will be determined and used to analyze electron conduction through molecules (e.g., octanedithiol) connected between gold electrodes. The form of the complex band structure clearly elucidates the molecule length dependence of the tunneling current and also suggests the energy for alignment of the Fermi level.

DOI: 10.1103/PhysRevB.65.245105 PACS number(s): 85.65.+h, 73.40.Gk, 73.63.Nm, 73.40.Ns

I. INTRODUCTION

The goal in the emerging field of molecular electronics is to create devices based on electronic current passing through a single molecule or an assembly of molecules. Low cost and small size are strong motivators that have rapidly advanced this field. Typical structures consist of a molecular film, or of a single molecule, sandwiched between a pair of metal contacts.[1–4] The Fermi level of the metal contacts usually lies between the highest occupied molecular orbital (HOMO) and lowest unoccupied molecular orbital (LUMO) electronic states of the molecule. A small applied voltage results in electron transport through the molecule via nonresonant tunneling or, for higher voltages, via resonant tunneling through a molecular energy level.[5,6] The nonresonant tunneling probability is quantified by a "β" parameter, where the tunneling probability is proportional to $e^{-\beta L}$, and L is the length of the molecule. The molecular orbital energies and wave functions control β, and general statements about its value are difficult to make.

A simplification exists for molecular systems that are constructed of a finite set of repeating building blocks. For these molecules, the methods of solid-state physics can be used to make predictions about β. The theory of complex band structures, originally developed to examine surface states of crystals, is used in this work to determine propagating and nonpropagating (tunneling) states of infinite repeating chains at any energy E. This analysis will yield β values that give reliable estimates of how the electron wave functions in the metal decay through a molecule that is a fragment of the infinite chain. The basic concept has been used previously in its simplest form by Beratan and Hopfield[7] to analyze electron tunneling rates through ruthenium dithiaspiro complexes. Expressions for decay rates of gap states in some model systems in molecular electronics have been derived by Magoga and Joachim[8] and Girard *et al.*[9] The exponentially decaying states have also been observed directly with a scanning tunneling microscope (Langlais *et al.*[10]).

In this paper, we examine infinitely long periodic one dimensional organic chains, for which finite fragments are the molecules of interest. Examples we examine in this work are shown in Fig. 1. They are [Fig. 1(a)] alkane chains with carbon single bonds, [Fig. 1(b)] alkene chains with alternating carbon double-single bonds, and [Fig. 1(c)] molecules formed from benzene rings linked by triply bonded carbon atoms. These examples are model molecules for molecular electronic studies.

The electron energy eigenstates in a periodic system can be taken to have the Bloch form

$$\psi(x) = e^{ikx}u(x),$$

where $u(x)$ is a function with the periodicity of the lattice. Normally, only real values of the Bloch k vector are considered since, for infinite systems, imaginary k solutions exhibit the physically unreasonable behavior of blowing up exponentially in some direction. The energy eigenvalues considered as a function of real k values (the band structure) reveal the detailed nature of electron transport through extended states in the material.

Imaginary (or complex) k solutions are also physically relevant and important for systems of finite size or, more generally, systems which contain breaks or defects in spatial uniformity. The simplest example is the transport of a free electron over a square potential energy barrier. Here the eigenstates are of the form e^{ikx} where k, a function of the

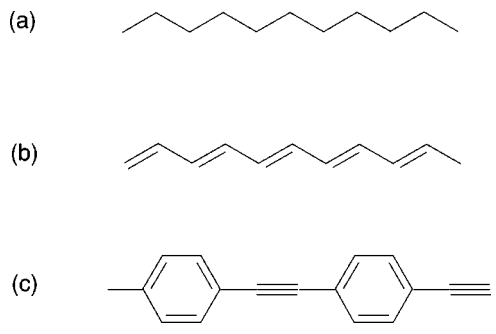

FIG. 1. Three organic periodic molecules.

electron energy, is real or imaginary depending on whether the electron energy is above or below the height of the potential energy barrier. Low energies lead to imaginary k, and the transmission probability (obtained from the square of the wave function) is approximately proportional to $e^{-\beta L}$ where L is the length of the barrier and $\beta=2|k|$. In this example, the function β(E) is $2\sqrt{2m(\phi-E)/\hbar^2}$, where ϕ is the height of the energy barrier. Just as the function $\beta(E)$ is important for tunneling through the barrier, so is the form of the complex band structure for a finite fragment (molecule) of an infinite chain.

A concise picture of electron transport through a rigid finite molecule is obtained from the complex band structure, which generalizes the usual band structure to include complex Bloch vectors. A fundamental assumption used here is that the interior of the molecule has a local environment very near that of the infinitely long ideal chain. Even if the ends are altered due to charge rearrangement, we assume that this has little effect on the atoms in the central region so that locally the Hamiltonian is that of the infinite molecule. As the molecule is lengthened, the central region lengthens, and an accurate measure of the reduction of tunneling is obtained from an analysis of the infinite chain.

Much of the previous work in molecular electronic has focused on current-voltage characteristics.[1,11–13] These are sensitive to a number of variables not directly related to the molecule (the nature of the contacts, the connection, the temperature, the chemical environment, etc.). An advantage of the complex band structure approach applied to a molecule is that it reveals aspects of conduction which are unique to the molecule, independent of the environment.

In this paper, we describe a method for obtaining the complex band structure of a molecule and apply it to some simple systems. We emphasize that the concept of a Bloch wave vector is only meaningful for a molecule which is a sequence of repeating units; hence we are restricted to molecules constructed by stacking repeating building blocks. This includes a wide variety of molecules, including (n-)alkanes, alkenes, alkynes, carbon nanotubes, polyester, polyanaline, and synthetic DNA (e.g., poly-A–poly-T). In Sec. II, we compute the complex band structure for a simple model system to illustrate the method and concepts, and obtain analytic formulas that serve as model formulas for more complex systems. In Sec. III we develop the theoretical techniques to compute the complex band structure following the method of Chang and Shulman.[14] In Sec. IV, we apply this to the case of n-alkanes. In Sec. V, we discuss the lineup of the Fermi level of Au for an n-alkane (octanedithiol) system. In Sec. VI we evaluate the complex band structure of an alkene chain and of a molecule formed from linked benzene rings. Finally, in Sec. VII we conclude.

II. EXAMPLE

Before presenting the complex band structure of a realistic system and a general method for computing complex band structures, it is instructive to determine the complex band structure of a simple model system.

The model we have chosen is a one-dimensional periodic arrangement of two types of atoms A and B, arranged in an alternating sequence $ABABABAB\ldots$. The unit cell consists of an A and a B atom and the spacing between cells is a (the distance between A and B is $a/2$). A two-band model of this kind has been analyzed previously.[15,9] The wave function in unit cell m is expressed as a linear combination of orthonormal orbitals ϕ_A and ϕ_B on each atom in that cell:

$$\Psi^{(m)}=C_A^{(m)}\phi_A+C_B^{(m)}\phi_B. \tag{1}$$

The Hamiltonian matrix has coupling $-t$ between orbitals on nearest-neighbor atoms only and the onsite energies are E_A and E_B, with $E_A<E_B$.

Assuming the Bloch form for the eigenstates, $C^{(m)}=e^{ikma}C^{(0)}$, the energy eigenvalues are found to be

$$E_{\pm}(k)=\Sigma\pm\sqrt{\Delta^2+2t^2(1+\cos ka)}, \tag{2}$$

where

$$\Sigma=\frac{E_A+E_B}{2}$$

and

$$\Delta=\frac{E_B-E_A}{2}.$$

The eigenvalues are shown in Fig. 2 for real and imaginary k values. The band gap in this model is $2|\Delta|$, and the valence-band top E_v $(=E_A)$ and conduction-band minimum E_c $(=E_B)$ occur at $\Sigma-|\Delta|$ and $\Sigma+|\Delta|$, respectively. The two bands (or branches) $E_+(k)$ and $E_-(k)$ are connected in

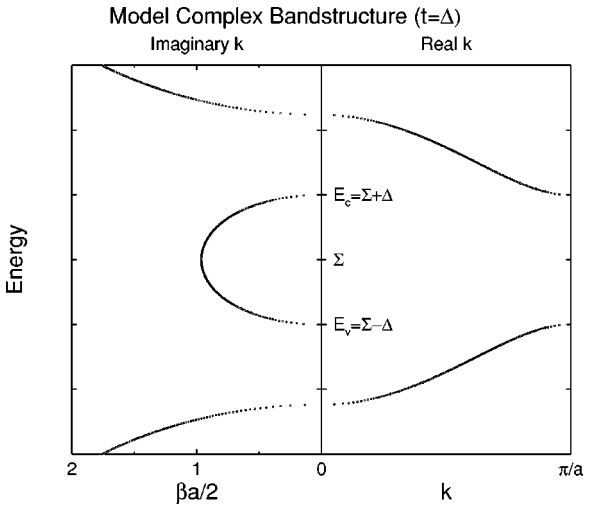

FIG. 2. The complex band structure for the model system, with t set equal to Δ. The right half of the figure is the usual (real k) band structure while the left region is a plot of $|\mathrm{Im}\,k|$ for the k solutions with an imaginary part. The valence-band branch (maximum at E_v) is connected to the conduction-band branch (minimum at E_c) at the branch point located at $E=\Sigma$. The k solutions with a nonzero imaginary part decay by $e^{-|\mathrm{Im}(k)|a}$ from one unit cell to the next. Of more direct significance is the reduction in the tunneling probability, $e^{-2|\mathrm{Im}(k)|a}=e^{-\beta a}$. This defines the quantity $\beta(E)=2\,\mathrm{Im}\,k(E)$.

the complex k plane at the branch point at $E=\Sigma$. The branch point occurs when $E_+(k)=E_-(k)$,[16,17] which requires

$$\Delta^2+2t^2(1+\cos ka)=0;$$

this can only be satisfied if $\cos ka<-1$, so k must have an imaginary component.

The imaginary k region of the band structure determines how an electron with a given energy will tunnel through a finite region of the crystal. In the gap region, between $\Sigma-\Delta$ and $\Sigma+\Delta$ (see Fig. 2), $|k|$ gives the rate of decay of the wave function from one cell to the next. As the energy approaches the band edge from the gap, $|k|$ decreases so an electron with an energy in the gap will tunnel more effectively as its energy approaches the band edge. The band edges each act as the top of an effective potential barrier; like the top of the simple square barrier, they mark the crossover point from decaying states to propagating ones.

We can find the complex k vector for energies in the gap from Eq. (2) by replacing $E_\pm$ by an input energy E and solving for $\cos ka$. The result is

$$\cos ka=-\gamma(E), \tag{3}$$

where

$$\gamma(E)=\frac{(E-E_v)(E_c-E)}{2t^2}+1. \tag{4}$$

The k solutions split off of the real axis from the band edges at $ka=\pi$. Writing $ka=\pi+i\beta(E)a/2$ we have

$$\beta(E)a/2=\ln[\gamma(E)+\sqrt{\gamma(E)^2-1}]. \tag{5}$$

The eigenstates in the gap change sign ($e^{i\pi}$) and decay by $e^{-\beta a/2}$ from one cell to the next. The corresponding decay in the probability ($|\psi|^2$) is $e^{-\beta a}$.

To make contact with tunneling through a barrier, we note that t^2 can be related to the effective mass m^*, $[(1/\hbar^2)d^2E/dk^2]^{-1}$, evaluated at the band edge. Expanding Eq. (2) for energies near the top of the valence band or the bottom of the conduction band yields

$$\frac{\hbar^2E_g}{2m^*a^2}=t^2. \tag{6}$$

Replacing t^2 by this effective mass expression in Eq. (5) for $\gamma(E)$ gives

$$\beta(E)=2\sqrt{\frac{2m^*}{\hbar^2}(E-E_v)} \tag{7}$$

for energies E near E_v and

$$\beta(E)=2\sqrt{\frac{2m^*}{\hbar^2}(E_c-E)} \tag{8}$$

for energies near E_c. These expressions are similar to the simple barrier tunneling expression

$$\beta(E)=2\sqrt{\frac{2m}{\hbar^2}(\phi_B-E)}, \tag{9}$$

where ϕ_B is the barrier height and E is the energy below the barrier.

We can take another approach to this problem using the (forward propagating) Green's function

$$G(E)=\sum_n\frac{|n\rangle\langle n|}{E-E_n+i\eta}. \tag{10}$$

The sum is over all eigenstates $|n\rangle$ of the system (each with eigenvalue E_n) and the limit $\eta\to 0+$ is to be taken. $G(E)$ is related to the propagator $G(t)=\Sigma_n|n\rangle e^{-iE_nt/\hbar}\langle n|$ by

$$G(t)=-\frac{1}{2\pi i}\int_{-\infty}^{\infty}G(E)e^{-iEt/\hbar}dE.$$

$\langle x'|G(t)|x\rangle$ is the probability amplitude for propagation from point x to x' in time t (>0) and we see that this is the sum of time-independent amplitudes $\langle x'|G(E)|x\rangle$ multiplied by time-dependent phases $e^{-iEt/\hbar}$. Loosely speaking, $G(E)$ indicates how electrons with energy E ''penetrate'' from one point (or state) to another.

For a one-dimensional periodic system with spacing a between unit cells, the cell-averaged Green's function[21] is defined as

$$G(m,E)=\int_{\text{cell}}\langle x+ma|G(E)|x\rangle dx$$
$$=\frac{1}{N}\sum_{nk}\frac{e^{ikma}}{E-E_{nk}+i\eta}. \tag{11}$$

Here m labels a unit cell, n is a band index, k varies over the entire Brillouin zone, and $N\to\infty$ is the number of cells in the system. For our model, this can be directly evaluated using contour integration. The result, in the gap region, is

$$G(m,E)=(\Sigma-E)\frac{[-\gamma(E)+\sqrt{\gamma(E)^2-1}]^m}{t^2\sqrt{\gamma(E)^2-1}}, \tag{12}$$

where $\gamma(E)$ is the same as in Eqs. (3) and (4). Writing $ka=\pi+i\beta a/2$ as before, this can be written as

$$G(m,E)=(\Sigma-E)\frac{(-1)^me^{-\beta ma/2}}{t^2\sinh\beta a/2}. \tag{13}$$

The (cell-averaged) Green's function $G(m,E)$ has the same exponential decay at energy E as the complex k Bloch states.

We make this connection because the cell-averaged Green's function is relevant to another important aspect of molecular conduction. As will be discussed further in Sec. V, when a molecule is connected between metal contacts, the tunneling electrons are those located at or near the Fermi level of the metal. In order to understand electron transport through the molecule it is necessary to estimate where the metal Fermi level lies relative to the molecule energy levels. The cell-averaged Green's function gives such an estimate.

The situation is similar to a Schottky barrier where an exchange of charge between the semiconductor and the metal—resulting in the formation of an interface dipole—brings the Fermi levels of the two materials into coincidence. A central problem in characterizing a Schottky barrier is to determine the location of the Fermi level relative to the semiconductor band edges near the interface.[18]

For the metal-semiconductor interface, there are metal-induced gap states[19] (MIGS) in the semiconductor gap region which decay exponentially in the semiconductor. These correspond to the Bloch states of the semiconductor which have k vectors with an imaginary component. There is an associated charge neutrality level ϕ_0 (Refs. 20–22) for the MIGS and it is expected that if the density of MIGS is reasonably large, the Fermi level should be ''pinned'' to ϕ_0. The effect may be viewed as a feedback mechanism where electrons leaking out of the MIGS and partly into the depletion region of the semiconductor cause further band bending which counters the whole process by lowering the energies of the MIGS.[23]

One particularly simple approach to the Schottky barrier problem was proposed by Tersoff,[21] who gave a prescription for determining ϕ_0 which is based only on the properties of the semiconductor. Tersoff proposed that the charge neutrality level should be located at the branch point in the gap of the complex band structure of the semiconductor. More specifically, since there may be more than one branch point in the gap, the ϕ_0 branch point is the branch point in the gap for Bloch k states which penetrate deepest ($|\mathrm{Im}\,k|$ smallest).

The method suggested by Tersoff for locating this branch point uses the cell-averaged Green's function. It follows from Allen[24] that the cell-averaged Green's function in the gap may be written as

$$G(m,E) = -ai \sum_{kn} \frac{e^{ikma}}{v(k,n)}, \tag{14}$$

where the sum is over *only* those values of k and n which satisfy both $E(k,n)=E$ and $\mathrm{Im}\,k\,\mathrm{sgn}(m)>0$. The restriction on $\mathrm{Im}\,k$ picks out the decaying solutions and excludes those which increase exponentially as $|m|$ increases. The quantity $v(k,n)$, the velocity times $\hbar$, is given by

$$v(k,n) = \frac{dE(k,n)}{dk}. \tag{15}$$

For the model system of this section,

$$v(k,n) = \frac{-t^2 a \sin ka}{E-\Sigma}, \tag{16}$$

k is given by Eq. (3), and application of Eq. (14) will yield Eq. (13) for the cell-averaged Green's function. The method for locating the branch point for the most penetrating gap states follows by recognizing that the contributions to $G(m,E)$ from each k value in the sum will vanish rapidly as m increases, so

$$G(m,E) \rightarrow -ai \frac{e^{ik_0 ma}}{v(k_0)} \quad \text{as } m \text{ increases}, \tag{17}$$

where k_0 has the smallest imaginary part of those k's in the sum.

We now have all the necessary tools using the MIGS theory to make an estimate of the position of the Fermi level of a metal contact relative to the LUMO-HOMO levels (roughly E_c and E_v, respectively) of the molecule. The energy of the branch point is the charge neutrality level ϕ_0 of the molecule. Physically this means the character of the state changes from valence (bonding) to conduction (antibonding) (Ref. 25) and the charge-neutrality point is where the energies of these two states are equal ($E_+ = E_-$ in our simple model). The Fermi level is pinned to this level in the MIGS theory. The branch point ϕ_0 determined by Tersoff is located at the energy where $G(m,E)=0$ (for large enough m). This follows from Eq. (17) since $v(k_0)=dE/dk$ is infinite at the branch point.

One can see from our model using Eq. (13) that the cell-averaged Green's function indeed vanishes at $E=\Sigma$, the branch point energy. This energy is the estimate of the pinning position of a metal Fermi level due to MIGS. Using this model and the complex band structures of organic molecules we consider below, it is a simple matter to obtain the branch points without evaluating the cell-averaged Green's function. As in Fig. 2, we simply seek a ''vertical'' region (i.e., $dE/dk \rightarrow \infty$, giving $G=0$) for an imaginary k value ($\beta/2$) at an energy E in the gap. This locates the branch point and, hence, an approximate estimate for the position of the metal Fermi level.

The Fermi level problem for the metal-molecule system will be examined in more detail in Sec. V. We note that the MIGS theory has had reasonable success in giving estimates of the Fermi level alignment of metal/semiconductor interfaces. A complete self-consistent calculation is necessary to obtain a more reliable value, assuming that defects do not influence the barrier.[26] We view the MIGS method applied to molecular electronic applications as simply a first approximation. In molecular electronics applications one would ideally want a single molecule between metal contacts, and the MIGS theory is based on planar interfaces in which charge transfer effects yield energy offsets similar to a parallel plate capacitor. In practice, many molecular electronics devices do in fact involve a planar array of contacts which arise from self-assembled monolayers (SAM's) and for these systems the assumptions built into the MIGS theory are closer to being correct.

III. METHOD TO DETERMINE THE COMPLEX BAND STRUCTURE

In this section we present a method for determining a complex band structure. In particular, we derive a mathematical technique which produces all Bloch k vectors (possibly complex) corresponding to a given input energy E. A sweep over a range of energies then reveals the complex band structure. An understanding of the method is not required for understanding complex band structures, however, so the reader may wish to skip this section.

A conventional band structure is obtained by choosing real k values and solving the energy eigenvalue problem

from the Hamiltonian. The loci of associated eigenenergies E are collected to produce the well-known $E(k)$ band structure. An alternative approach, which is more complete but less direct, is to instead consider the energy as input and obtain as output the k values that produce that energy. This ''inverted'' procedure produces k values that may have both real and imaginary parts, and this generates the complex band structure.

The goal in obtaining a complex band structure is to obtain the spectrum of k's associated with any real energy E. This inverted approach has a long history, and the theoretical methods used are generally referred to as transfer matrix techniques.[27] The technique can be applied using local-atomic-like orbitals[28,29,14] or plane-wave basis sets.[30–32] In the present case we use a set of local atomic orbitals as our basis.

The specific theoretical approach we have taken follows from the general theory developed by Chang and Shulman (CS).[14] The concept is to rewrite the Schrödinger equation as an eigenvalue equation in λ, where $\lambda = e^{ika}$ ($a =$ lattice constant). The eigenvalues λ are to be determined for any given input energy E. When an output eigenvalue satisfies $|\lambda| = 1$, we have a real k value; when λ is off the unit circle, we have exponentially decaying or growing (tunneling) solutions corresponding to complex k values. It is these tunneling solutions that reduce the transmission in molecular electronic systems and, hence, are of special interest.

We define an operator Z (a matrix) as $Z = (H - ES)$ where H is the Hamiltonian, S is the overlap matrix between nonorthogonal atomic orbitals, and E is the input scalar energy of interest. The Schrödinger equation is written as

$$\sum_{m=-N}^{N} Z^{(m)} \vec{C}^{(m)} = 0, \tag{18}$$

where $Z^{(m)} = H^{(m)} - ES^{(m)}$. The matrices $H^{(m)}$ and $S^{(m)}$ contain the (Hamiltonian and overlap) matrix elements between the orbitals of the zeroth and mth unit cells. The sum over m is the sum over unit cells which interact through Hamiltonian matrix elements or orbital overlaps with a chosen (the zeroth) unit cell. Electronic states are linear combinations of atomiclike orbitals, and the vector $\vec{C}^{(m)}$ contains the coefficients of the basis orbitals in cell m. Interactions are included from the central cell to cells N lattice constants away.

The periodicity of the system permits us to invoke a generalization of Bloch's theorem that relates vectors on neighboring cell,

$$\vec{C}^{(m+1)} = \lambda \vec{C}^{(m)}. \tag{19}$$

One can repeatedly insert Eq. (19) into Eq. (18) and obtain a matrix polynomial equation for λ up to order λ^{2N}. This is difficult to solve. Instead, in the method of CS, a new matrix of larger size is created (a transfer matrix), with the ultimate goal of producing a linear polynomial in λ; a linear polynomial is tantamount to an eigenvalue equation for λ, which can be solved by standard algorithms. From Eqs. (18) and (19) we obtain the following set of $2N$ equations:

$$-\sum_{m=-N}^{N-1} Z^{(m)} \vec{C}^{(m)} = Z^{(N)} \lambda \vec{C}^{(N-1)}, \tag{20}$$

$$\vec{C}^{(m+1)} = \lambda \vec{C}^{(m)} (-N < m < N-2). \tag{21}$$

When $Z^{(N)}$ is nonsingular (i.e., its inverse exists) one can multiply the first of these equations by $(Z^{(N)})^{-1}$ to yield a simple eigenvalue problem for λ. The transfer matrix generated by Eqs. (20) and (21) can then be written in matrix form as

$$\begin{pmatrix} -[Z^{(N)}]^{-1}Z^{(N-1)} & -[Z^{(N)}]^{-1}Z^{(N-2)} & \cdots & -[Z^{(N)}]^{-1}Z^{(-N+1)} & -[Z^{(N)}]^{-1}Z^{(-N)} \\ 1 & 0 & \cdots & 0 & 0 \\ 0 & 1 & \cdots & 0 & 0 \\ \vdots & \vdots & & \vdots & \vdots \\ 0 & 0 & \cdots & 1 & 0 \end{pmatrix} \begin{pmatrix} \vec{C}^{N-1} \\ \vec{C}^{N-2} \\ \vdots \\ \vec{C}^{-N+1} \\ \vec{C}^{-N} \end{pmatrix} = \lambda \begin{pmatrix} \vec{C}^{N-1} \\ \vec{C}^{N-2} \\ \vdots \\ \vec{C}^{-N+1} \\ \vec{C}^{-N} \end{pmatrix}. \tag{22}$$

Unfortunately, in all but the simplest of models, the matrix $Z^{(N)}$ is singular, and the matrix $[Z^{(N)}]^{-1}$ does not exist. Matrix elements between orbitals go to zero (or effectively so) past the sum of their orbital ranges. If any orbital within cell N has no interaction with any orbital in cell ''zero,'' the matrix $Z^{(N)}$ will have a row of zeros and the matrix is singular. In large unit cells this is likely to occur since atoms near the mutual boundary between the two cells are much closer than a pair of atoms each located on opposite sides. We now describe a general method to easily identify and remedy this problem.

Our method is based on identifying two subspaces: a ''range'' subspace and a ''null'' subspace. When $Z^{(N)}$ is singular, it can rigorously be decomposed as $Z^{(N)} = UW_D V^{\dagger}$ where U and V are unitary matrices and W_D is diagonal. This is the well-known singular value decomposition (SVD).[33] Defining $\vec{D}^{(m)} = V^{\dagger}\vec{C}^{(m)}$ and $Y^{(m)} = U^{\dagger}Z^{(m)}V$ we obtain replacements of Eqs. (20) and (21):

$$-\sum_{m=-N}^{N-1} Y^{(m)}\vec{D}^{(m)} = W_D \lambda \vec{D}^{(N-1)}, \tag{23}$$

$$\vec{D}^{(m+1)} = \lambda \vec{D}^{(m)} (-N < m < N-2). \tag{24}$$

In a SVD, that which is producing the singularity is clearly identified and is visible as a null submatrix of W_D. We arrange the columns of U and V so that W_D has the form

$$W_D = \begin{pmatrix} w_D & 0 \\ 0 & 0 \end{pmatrix},$$

where w_D is a diagonal matrix with all nonzero diagonal values. The null matrix in the lower right-hand corner of W_D defines the null subspace, and the subspace spanned by w_D defines the range subspace. To simply treat these two subspaces, we define projector operators in the range and null subspaces, I_R and I_N, respectively. The range projector I_R is a diagonal matrix with diagonal values of 1 or 0. The values of 1 are given to those elements in the same subspace as w_D and a zero is assigned to elements in the same subspace as the null matrix in the lower right-hand corner of W_D. In other words, I_R is obtained from W_D by replacing each (diagonal) elements of w_D with a 1. The null space projector I_N is the identity matrix minus I_R. We also define a matrix W by $W = W_D + I_N$; this matrix, unlike W_D, is invertible.

The strategy is to replace Eq. (23) by two sets of equations, instead of one. One set of equations applies to the range subspace and the other to the null subspace. We first rewrite Eq. (23) using $W_D = W - I_N$ and $W^{-1} I_N = I_N$, so that Eq. (23) can be written as

$$-W^{-1}\sum_{m=-N}^{N-1} Y^{(m)}\vec{D}^{(m)} = \lambda \vec{D}^{(N-1)} - I_N \lambda \vec{D}^{(N-1)}. \tag{25}$$

Equation (25) is the equation we use to develop the two sets of equations for the range and null subspaces.

The range subspace rows of Eq. (25) are easy to determine. We multiply by I_R and use $I_R I_N = 0$ to yield

$$-I_R W^{-1}\sum_{m=-N}^{N-1} Y^{(m)}\vec{D}^{(m)} = \lambda I_R \vec{D}^{(N-1)}. \tag{26}$$

This equation involves $I_R \vec{D}^{(N-1)}$ on the right, which is the vector in the range subspace.

The more complex case is that of the null subspace, with equations involving $I_N \vec{D}^{(N-1)}$ on the right. This is accomplished in four steps. In the first step, we multiply Eq. (25) by $W \lambda I_N$. The right-hand side vanishes since $I_N I_N = I_N$, and using $[W, I_N] = 0$, we obtain $I_N \Sigma_{m=-N}^{N-1} Y^{(m)} \lambda \vec{D}^{(m)} = 0$. Using Eq. (24), this sum is rewritten to expose the $D^{(N-1)}$ term as

$$I_N \sum_{m=-N}^{N-2} Y^{(m)}\vec{D}^{(m+1)} + I_N Y^{(N-1)} \lambda \vec{D}^{(N-1)} = 0.$$

In the second step, the identity in the form $I_R + I_N$ is inserted in front of $\vec{D}^{(N-1)}$,

$$I_N \sum_{m=-N+1}^{N-1} Y^{(m-1)}\vec{D}^{(m)} + I_N Y^{(N-1)} I_R \lambda \vec{D}^{(N-1)} + I_N Y^{(N-1)} I_N \lambda \vec{D}^{(N-1)} = 0. \tag{27}$$

In the third step we use $y^{(N-1)}$, which is the null subspace part of $Y^{(N-1)}$ contained in $I_N Y^{(N-1)} I_N$. This matrix is augmented to the full space by defining a matrix Q as

$$Q = I_N Y^{(N-1)} I_N + I_R. \tag{28}$$

The matrix Q is simply the identity in the range subspace and the matrix $y^{(N-1)}$ in the null subspace and is of the form

$$Q = \begin{pmatrix} I & 0 \\ 0 & y^{(N-1)} \end{pmatrix}. \tag{29}$$

In the fourth and final step, we use $Q I_N = I_N Y^{(N-1)} I_N$ in the third term of Eq. (27) and use Eq. (26) in the second term to finally obtain $\vec{D}^{(N-1)}$ in the null subspace,

$$I_N\left(\sum_{m=-N+1}^{N-1} Y^{(m-1)}\vec{D}^{(m)} - Y^{(N-1)} I_R W^{-1} \sum_{m=-N}^{N-1} Y^{(m)}\vec{D}^{(m)}\right) = -Q\lambda I_N \vec{D}^{(N-1)}. \tag{30}$$

If the submatrix $y^{(N-1)}$ in Eq. (29) is invertible, so is Q and Eq. (30) multiplied by $-Q^{-1}$, together with Eq. (25) and (24), makes up a complete eigenvalue problem:

$$-I_R W^{-1}\sum_{m=-N}^{N-1} Y^{(m)}\vec{D}^{(m)} = \lambda I_R \vec{D}^{(N-1)},$$

$$-I_N Q^{-1}\left(\sum_{m=-N+1}^{N-1} Y^{(m-1)}\vec{D}^{(m)} - Y^{(N-1)} I_R W^{-1}\sum_{m=-N}^{N-1} Y^{(m)}\vec{D}^{(m)}\right) = \lambda I_N \vec{D}^{(N-1)},$$

$$\vec{D}^{(m+1)} = \lambda \vec{D}^{(m)} (-N < m < N-2). \tag{31}$$

Equations (31) can be assembled into matrix form as in Eq. (22) to produce an eigenvalue equation for λ for a given E, which can be solved numerically and completes the task. If the situation is unusual and the submatrix $y^{(N-1)}$ is not invertible, then the procedure for handling singular $Z^{(N)}$ can be repeated for $y^{(N-1)}$. We did not encounter this difficulty in the present work.

IV. COMPLEX BAND STRUCTURE FOR AN ALKANE

Perhaps the most studied self-assembled monolayer system in nanotechnology is that of the *n*-alkanes[34,35] (see Ref. 35 for many references). The *n*-alkanes $CH_3(CH_2)_N CH_3$ are nonbranching chains of singly bonded carbon atoms. Thiolated alkanes $CH_3(CH_2)_N SH$ spontaneously assemble into highly ordered monolayers on a gold (111) surface. The strong Au-S bond cleaves the terminal hydrogen, creating a film of van der Waals interchain-bonded molecules.[36] The

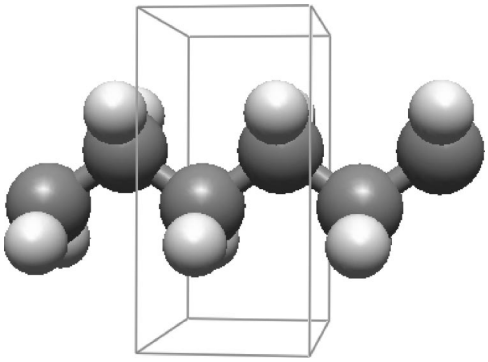

FIG. 3. The structure of an infinite alkane chain. The structure is ideal with all bonding angles 109.47°. Three repetitions of the unit cell are shown.

chain exists in any desired length N, with a typical film in molecular electronic applications having N in the range of 8–20.

The I-V characteristics of the alkanes themselves can be measured with, for example, a conducting atomic force microscope.[37] Alkane monolayers also serve as a convenient supporting, insulating matrix in which other molecules can be embedded and their conducting properties measured. Recent experiments have been performed in which a low concentration of alkanedithiol molecules are embedded in a monothiol SAM. Contact at the other end of the dithiols is made with gold nanoparticles and single-molecule tunneling through the alkanedithiols is observed.[2]

Tunneling through an alkane thiol or dithiol film will be very sensitive to the length of the alkane chain. One theoretical approach is to investigate each molecule individually and determine the tunneling probability. In the complex band structure approach used here, we consider only the infinite-length alkane chain and the tunneling characteristics are determined by the complex k vectors that produce decaying wave functions. The major assumption is that the electronic states of the finite-length molecule are a subset of the infinite-chain states. This means that the finite length does not create any intrinsically new states, but rather produces only finite-size effects. An analogy is that the harmonics of a short violin string are a subset of those present in the vibrations of a very long string.

The atomic structure of the infinite-length alkane chain is shown in Fig. 3. The angles and bond lengths used are the ideal values: all angles are tetrahedral (109.47°), the C-C bond length is 1.54 Å, and the C-H bond length is 1.10 Å.

The conventional band structure (*real* k) for an infinite alkane chain is shown in Fig. 4. We use two different electronic structure techniques, both of which use density-functional theory and pseudopotentials. We use Fireballs-2000 (Ref. 38) using a minimal basis set (H has a single s state, C an sp^3), and SIESTA (Ref. 39) using an extended basis set (sp^3 for H, sp^3d^5 for C). The top of the valence band has been shifted so that it defines zero energy. Both methods give similar band structures, especially for the occupied valence states. Differences between the methods are more pronounced for the conduction states. In addition, the band gap is smaller for the extended basis than for the minimal basis calculation: 9.00 eV vs 10.25 eV. However, in density-functional theory, the band gap is usually underestimated. The experimental ionization potentials for n-alkanes are all approximately 10 eV.[40]

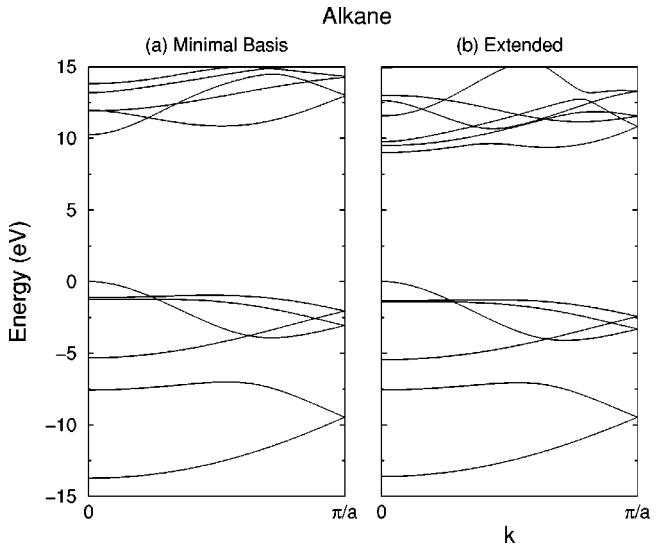

FIG. 4. The conventional band structure of an infinite alkane chain computed using (a) a minimal basis set (Ref. 38) and (b) an extended basis set (Ref. 39). Density-functional theory is used in both methods in the local density approximation. In both figures, the top of the valence band (HOMO) is defined to have zero energy. The k vector is real and goes from 0 to π/a, where "a" is the 1D lattice spacing.

We now examine the complex band structure for the alkane chain using the local orbital method described in Sec. III. We show the complex band structures calculated with the minimal basis set [Fig. 5(a)] and with the extended basis set [Fig. 5(b)]. In each figure, the region to the right of the origin shows the real parts of the k values obtained at each energy. The region to the left of the origin displays $\beta = \mathrm{Im}(ka)$. This quantity is proportional to the decrease of the tunneling probability per carbon [$2\,\mathrm{Im}(ka)$ is the decrease of the tunneling probability per cell, and there are two carbons per cell]. The transmission probability for an electron with a given β is then proportional to $e^{-\beta N}$ where N is the number of carbon atoms in the alkane.

In general k can have both real and imaginary parts. In this case, the state is not propagating and we only show the imaginary part of k which corresponds to the decay of the state. The rightmost panel shows k vectors that are entirely real. These energy-real k points reproduce the conventional band structure.

Let us focus our attention on the energies within the fundamental band gap region (between $E=0$ and ≈ 10 eV). The extended basis calculation has more structure for β than the minimal basis calculation. But this extra structure occurs for large β values and is loosely interpreted as decaying waves from distant bands. The large β values produce decaying states that have negligible tunneling probability after just a few C atoms. What is observed in experiment for chains with on the order of ten carbon atoms will be only those states with small β values. Comparing Figs. 5(a) and

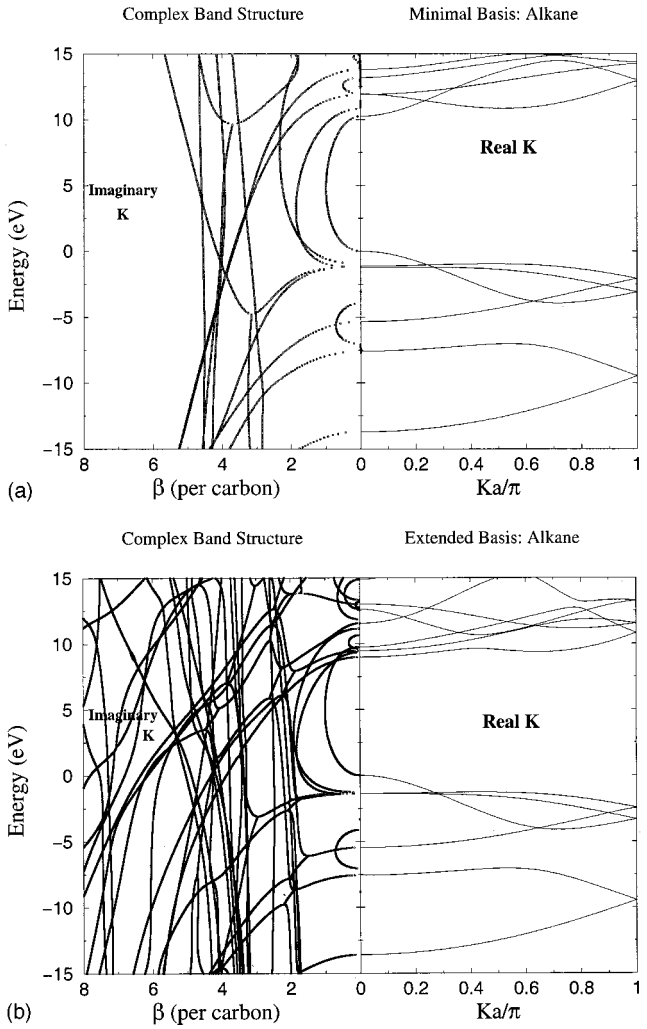

FIG. 5. The complex band structure for (a) a minimal basis set (Ref. 38) and (b) an extended basis set. The top of the valence band is set to 0 eV. The right panel shows $E(k)$ for k completely real, which is the conventional band structure. The left panel shows β (the imaginary part of the complex k solutions) for energies that have complex k vectors. The units of β shown are such that $e^{-\beta}$ is the reduction in the tunneling probability from one carbon atom to the next. Specifically, the decrease of the wave function is $e^{-\mathrm{Im}(k)a}$ per unit cell; the decrease in the probability is $e^{-2\,\mathrm{Im}(k)a}$ per unit cell, and since there are two carbon atoms per unit cell, the decrease in the probability per carbon is $e^{-\mathrm{Im}(k)a}$. Thus, in this particular plot, β is obtained from $\mathrm{Im}(k)a$.

5(b), we see that for these states both calculations give virtually identical behavior.

In the fundamental band gap, the smallest β values are given by a semielliptical-like curve similar to the model curve in Fig. 2. We do detect some difference between the two calculations for this semielliptical curve near the conduction band. In the extended basis system there are a couple of other β bands that pass through the semiellipse very near the conduction band. In fact, the extended basis calculation suggests that for energies very near the conduction band, there are three distinct β values that are all comparable and that can contribute to tunneling.

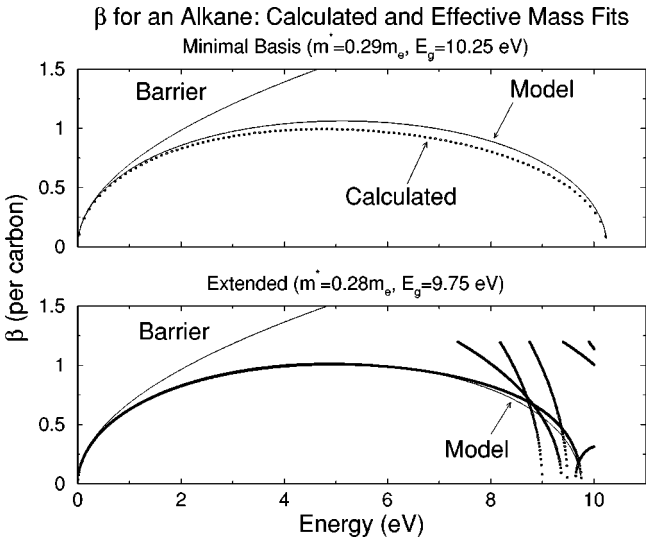

FIG. 6. The lowest β-value semielliptical curve for energies in the fundamental band gap region computed using a minimal basis set. For comparison, the model fit to expression Eq. (5) is shown. The two parameters E_g and m^* are obtained from the conventional band structure where m^* is the valence-band (hole) mass. The curves labeled ''Barrier'' are a barrier model [Eq. (7)] coming from the valence band.

Near the conduction band we must recognize that the tunneling may involve more than just one β value. Let us examine our results in more detail for energies in the band gap that are not near the conduction-band edge. We examine the single semielliptical curve for the minimal basis set. The extended basis set gives almost identical results.

The semielliptical band is shown in Fig. 6. We see that the tunneling probability, which goes as $e^{-\beta N}$, where N is the number of carbon atoms, has a β value near 1 at midgap and which decreases to zero as the energy approaches the conduction- (E_c) or valence- (E_v) band energies. A model expression of $\beta(E)$ can be obtained using Eq. (5) where $\gamma(E)$ is given by Eq. (4). A value for t is determined using Eq. (6) with the effective mass determined from the curvature of the valence-band; the value for E_g is taken as the energy difference between the valence-band edge and the edge of the associated unoccupied band it is joined to by the semielliptical β curve. In general, this unoccupied band is not necessarily the lowest in energy of the unoccupied bands. This is seen in the extended basis calculations [Fig. 5(b)] of the complex band structure where there are a few intervening unoccupied bands between the fundamental β semiellipse and the point at which it connects to an unoccupied band.

The two values E_g and m^* determine the model expression and this is also plotted in Fig. 6 for both the minimal and extended basis calculations. The agreement is very good. In the extended basis calculation the model curve is nearly indistinguishable from the calculated curve. Also shown are the simple barrier tunneling curves Eq. (7) using the valence-band effective mass. The barrier tunneling model is a reasonable approximations only for energies very close—within about 1 eV—to the band edge.

V. FERMI LEVEL LINEUP

The complex band structure specifies how an electron with a given energy will propagate through a molecule. If the molecule is connected between metallic electrodes, the conducting electrons are those with energies located near the Fermi level of the metal. To understand the conducting behavior of the molecule, it is therefore necessary to estimate the metal's Fermi level lineup with the molecule's band structure for the complete metal-molecule-metal system. For example, in the *n*-alkanes, we need to know where the Fermi level lies relative to the semiellipse of Fig. 6. The Fermi level or band lineup problem is central in the study of Schottky barriers and heterojunctions and has also received attention in molecular electronics.[41]

Assuming that Tersoff's branch point method remains valid for metal-molecule interfaces, we estimate that the Fermi level is located at the ϕ_0 branch point in the complex band structure as discussed in Sec. II. This branch point is identified as the energy where the slope dE/dk, becomes infinite for the most penetrating gap states—in other words, the point where the tangent to the β ellipse in the complex band structure becomes vertical. Specifically, in Fig. 5, this corresponds to the peak of the β ellipse where $\beta = 1.0$ per carbon.

A more rigorous determination of the position of the Fermi level can be performed by solving the entire metal-molecule electronic structure problem self-consistently. The Fermi level lineup is determined from the projected densities of states which reveal the relative location of the molecule energy levels. In particular, the most convenient and visible reference points are the HOMO (valence band) and LUMO (conduction band). We performed these calculations using a periodic geometry of alternating octanedithiol monolayers and gold (111) ''slabs'' as shown in Fig. 7. The gold slabs were chosen to be six layers thick. However, we have also performed calculations using up to 12 layers, and the results are very similar. The surface structure of the monolayer is $(\sqrt{3}\times\sqrt{3})R30°$ (see, e.g., Ref. 35), and the orientation of the octanedithiol molecule (one per unit cell) is described in Fig. 8. This orientation was determined by performing structural relaxations of the molecule with the gold atom positions fixed in an idealized configuration with an Au-Au bond length of 2.885 Å. However, while a preferred orientation of the molecule as a whole was estimated with structural relaxations, the C-*X* bond lengths and *X*-C-*X* bond angles were fixed at their ideal values: C-H = 1.10 Å , C-C = 1.54 Å, C-S = 1.84 Å, and *X*-C-*X* = 109.47°.

We performed calculations on two variations of this structure. These are shown in Fig. 9. In the first (a), the sulfur atoms were positioned 1.95 Å directly above a ''hollow'' in the gold surface, equidistant from three surface gold atoms. The S-Au bond length is then 2.56 Å. In the second structure (b), there is a gold atom (darkened in the figure) inserted between each S atom and the gold surface. The extra gold atoms sit in the ideal position above the hollow (Au-Au bond length = 2.885 Å). We used a S-Au bond length of 2.25 Å and an Au-S-C angle of 109.47°; these choices were guided by structural relaxations. Structures (a) and (b) will be called the S-hollow and the S-Au-hollow structures, respectively.

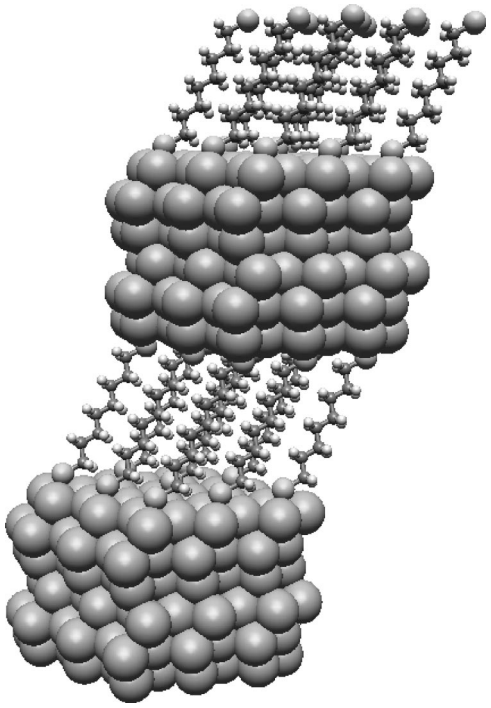

FIG. 7. The alternating layer structure used in the calculations of the density of states. The unit cell is shown repeated $3\times3\times2 = 18$ times.

We determined the Kohn-Sham (self-consistent) single-electron eigenstates and energies for this structure using minimal,[38] extended,[39] and plane-wave[42] basis sets. All methods used the same ideal geometry described. For the local orbital methods a $6\times6\times2$ Monkhorst-Pack grid was used for *k*-point sampling (6's for directions parallel to the gold surfaces and 2 for the gold-slab to gold-slab direction)

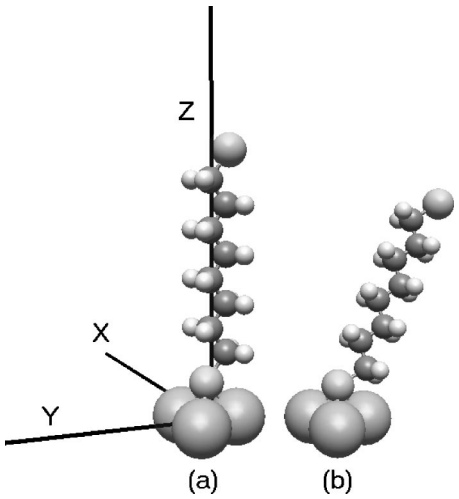

FIG. 8. Alignment of the octanedithiol chain with the Au (111) surface. Begin with orientation (a) in which the carbon backbone is in the *y*-*z* plane and perpendicular to the Au (111) surface (in the *x*-*y* plane). Rotate the molecule (in the right-handed sense) $-30°$ about the *z* axis, then 7° about the *y* axis, and finally 30° about the *x* axis. The result (b) is the orientation used in our calculations.

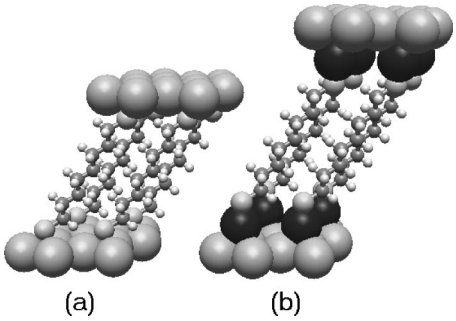

FIG. 9. The S-hollow structure (a) and S-Au-hollow structure (b) used in the density of states calculations. The only difference is the extra gold atom (darkened for emphasis) inserted between each sulfur and the gold surface.

and, for the plane-wave calculation, a $4\times4\times4$ grid was used.

Projected densities of states for the S-hollow structure are shown in Fig. 10. The projected density of states onto the orbitals of a ''middle'' carbon atom (fourth or fifth carbon from the end of the eight-carbon chain) is shown for each basis set. This reveals the position of the octane HOMO and LUMO levels and it is seen that—although the HOMO-LUMO gap is smaller for the extended and plane-wave calculations—in all three cases the Fermi level (defined as 0 eV) lies approximately in the middle of the HOMO-LUMO gap of the molecule. This is in agreement with the branch point estimate. Specifically, for the minimal basis, the MIGS theory predicts E_F to be about 5.4 eV above the HOMO of the octane chain and the self-consistent minimal basis calculation gives about 4.9 eV.

Some other features of the density of states (DOS) are shown for the minimal basis calculation. Here the DOS are also shown projected onto the sulfur orbitals and the neighboring or ''end'' carbon orbitals. It is important to note that there are prominent (localized) sulfur-based states in the middle of the alkane chain HOMO-LUMO gap. It may be that these states play a significant role in electron conduction, in particular for shorter alkanes. In the projected DOS for the end carbon, the alkane HOMO-LUMO levels are visible but they are blended with sulfur and gold states. These states are partially the tails of MIGS and their presence is the reason for focusing on the middle carbon atom where most of the MIGS have decayed away and the true HOMO and LUMO states are revealed. Similar features are seen in the projected DOS for the extended and planewave basis calculations.

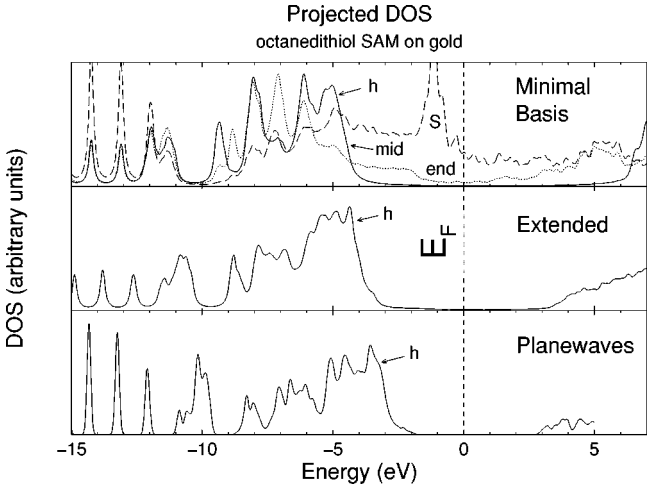

FIG. 10. Projected densities of states for the S-hollow structure [Fig. 9(a)] using three different electronic structure methods. The minimal basis panel shows the DOS projected onto a sulfur and onto a carbon at the end and at middle (mid) of the octane chain. The extended and plane-wave panels show only the projections onto a middle carbon atom. The Fermi level is at 0 eV. ''h'' indicates the approximate position of the alkane HOMO.

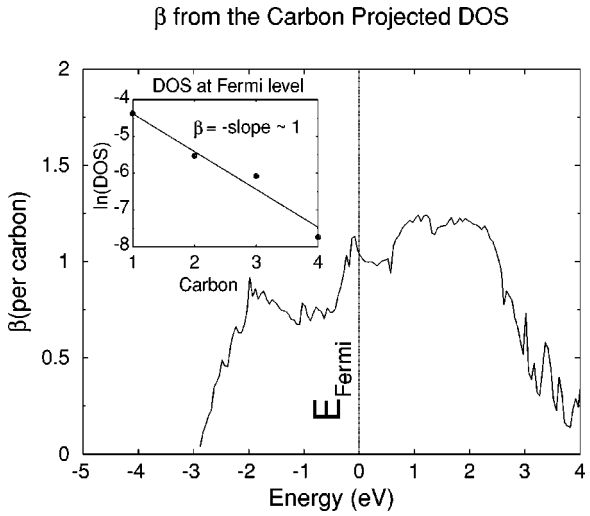

FIG. 11. The β curve determined from the densities of states projected onto carbon atoms 1, 2, 3, and 4 (counting from the end of the octane chain) of the octanedithiol SAM (S-hollow structure). The calculation was done using the DOS determined with plane waves and the result is similar to the β curves determined from the minimal and extended local orbital basis calculations. The slight dip near ≈ -1 eV is at the location of a state localized on the sulfur.

The decay in the MIGS component of the density of states from the end carbons to the middle carbons provides a direct and simple alternate way of calculating β. The projected DOS ρ_n on the nth carbon from the end contributed by the MIGS should be approximately given by

$$\rho_n(E)=\rho_0(E)e^{-\beta(E)n},$$

where $\rho_0(E)$ is a function of energy only. An estimate of $\beta(E)$ may then be determined by fitting, for each energy, the projected DOS on the carbons (as a function of carbon number n) to an exponential. This was done for the planewave calculation and the result is shown in Fig. 11. The β curve is noisy but still has a similar shape to the ideal β curves determined from the complex band structure calculations. One curious feature is the slight dip around -1 eV. This is the location of the sulfur state mentioned before.

Finally, the DOS projected onto the middle carbon for the S-hollow and S-Au-hollow structures are compared in Fig. 12. It is seen that the HOMO has shifted upward, towards the Fermi level, by just over 1 eV. This result is from a minimal

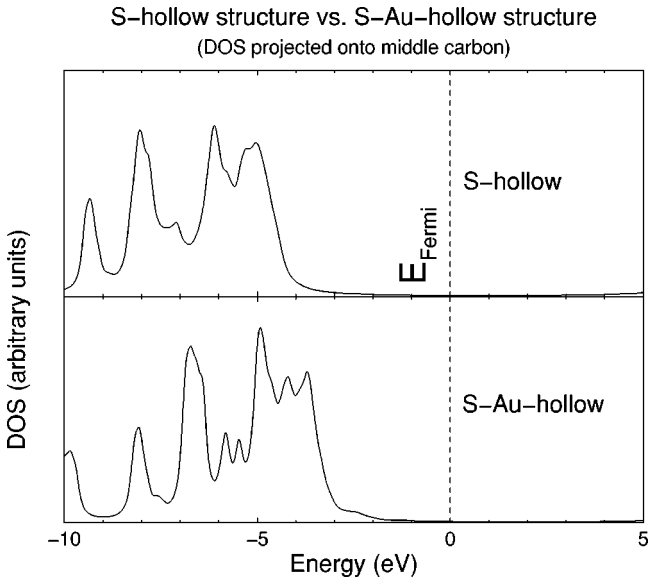

FIG. 12. The effect of the insertion of a gold atom between the S and gold surface (S-Au-hollow) using a minimal basis calculation. The HOMO is shifted upward by just over 1 eV compared to the S-hollow structure.

basis calculation, but the same trend is seen in both the extended basis and plane-wave calculations.

This result suggests that the Fermi level is sensitive to the structural details about the metal-molecule interface so that the branch-point estimate of the position of the Fermi level is only approximate. This underscores the difficulty of making reliable calculations of the current-voltage characteristics of a molecule where a small change in the position of the Fermi level is amplified by the exponential nature of the tunneling.

VI. COMPLEX BAND STRUCTURE OF ALKENE AND BENZENE CHAINS

In this section we present the complex band structures of two other organic molecules: an alkene chain and linked benzene rings.

The alkene structure has alternating single (1.54 Å) and double (1.34 Å) bonds [Fig. 1(b)]. The unit cell is $(CH)_2$. The alkene chain complex band structure is shown in Fig. 13. The band gap is very narrow, approximately 1.9 eV, and the valence-band edge occurs at $k=\pi/a$. The β values in the gap are much smaller than for the alkane. The peak β values in the gap for the alkane and alkene chains are $\beta=0.79$ Å^{-1} (about 1.0 per carbon) and $\beta=0.27$ Å^{-1} (about 0.34 per carbon), respectively. As expected, electron tunneling states in the gap are far more penetrating for the conjugated alkene structure.

Finally, the complex band structure of the linked benzene rings [Fig. 1(c)] is shown in Fig. 14. All C-C bond lengths are 1.39 Å except for the triple bond which is 1.2 Å. In the figure, β is in units of Å^{-1}. The band gap is 2.1 eV and the peak value for the β curve in the gap is coincidentally the same as for the alkene, $\beta=0.27$ Å^{-1}. There are several flat bands which presumably represent states localized on the benzene rings or the triple bonds.

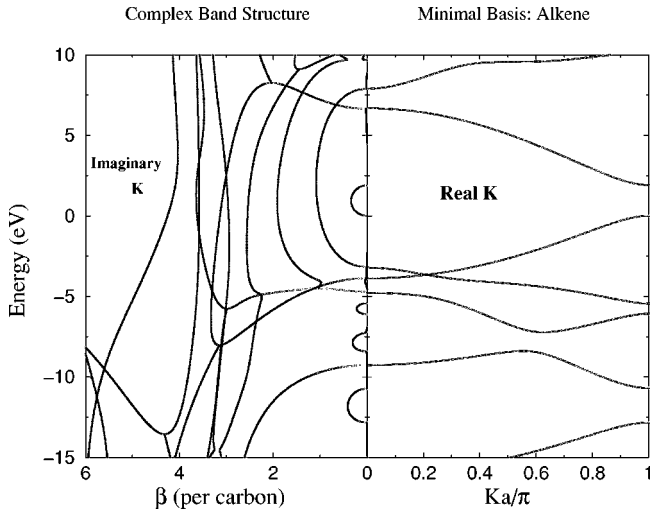

FIG. 13. The complex band structure for the infinite alkene [Fig. 1(b)]. The figure is as Fig. 5(a) for an *n*-alkane. The valence-band top is at 0 eV.

VII. CONCLUSION

In this paper the complex band structure has been a focal point for a number of important topics related to molecular conduction.

The complex band structure describes all the electronic Bloch states where the Bloch k vector ranges over the entire complex plane. The main advantage of the complex band structure is that it provides a clear picture of the nature of the electron states in the HOMO-LUMO gap region of the molecule. These are the electron tunneling states which determine the nature of electron transport through the molecule. The $\beta(E)$ curve, which describes the most penetrating of the gap wave functions, gives a simple quantitative measure of the rate of decay of these tunneling states and so reveals the expected length dependence of the conductivity.

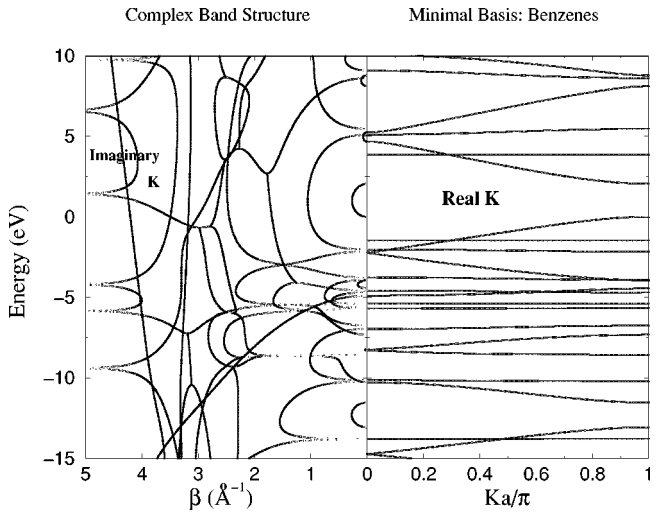

FIG. 14. The complex band structure for the linked benzene ring structure [Fig. 1(c)]. The units of β shown correspond to the probability decay per angstrom. The valence-band top is at 0 eV.

We have presented (Sec. III) a method for obtaining the full complex band structure of a periodic molecule. We have also described (Sec. V) a simple alternative method for obtaining $\beta(E)$ from projected densities of states. This method directly reveals the exponentially decaying electron wave functions—analogous to metal-induced gap states. This method generalizes to nonperiodic molecules.

Besides describing the form of the tunneling wave functions, the $\beta(E)$ semiellipse also provides a simple means for estimating the location of the Fermi level for a molecule in contact with a metal. In particular, according to Tersoff's theory,[21] the Fermi level for a Schottky barrier should be located near the peak of the $\beta(E)$ semiellipse. Applied to the metal-molecule system, this estimate was found to be in reasonable agreement with more elaborate electronic structure calculations of an octanedithiol monolayer connected to gold slabs (Sec. V). However, the location of the Fermi level was also found to be somewhat sensitive to structural details of the metal-molecule connection.

ACKNOWLEDGMENTS

We thank the National Science Foundation (NIRT ECS-0103175), (MRSEC DMR-96-32635), and (DMR-99-86706) for support. We would also like to thank the molecular electronics group at Arizona State University: Xiao Dong Cui, Ganesh Ramachandran, Jin He, Stuart Lindsay, Alex Primak, Xristo Zarate, Devins Gust, Anna Moore, Tom Moore, Salah Boussaad, Huixin He, Nongjian Tao, and, from Motorola, Gari Harris, Larry Nagahara, Alex Demkov, and X. Zhang.

[1] M. A. Reed, C. Zhou, C. J. Muller, T. P. Burgin, and J. M. Tour, Science **278**, 252 (1997).
[2] X. D. Cui, A. Primak, X. Zarate, J. K. Tomfohr, O. F. Sankey, A. L. Moore, T. A. Moore, D. Gust, G. Harris, and S. M. Lindsay, Science **294**, 571 (2001).
[3] D. Porath, A. Bezryadin, S. de Vries, and C. Dekker, Nature (London) **403**, 635 (2000).
[4] J. Chen, M. A. Reed, A. M. Rawlett, and J. M. Tour, Science **286**, 1550 (1999).
[5] V. Mujica, M. Kemp, A. Roitberg, and M. Ratner, J. Chem. Phys. **104**, 7296 (1996).
[6] W. Tian, S. Datta, S. Hong, R. Reifenberger, J. I. Henderson, and C. P. Kubiak, J. Chem. Phys. **109**, 2874 (1998).
[7] D. N. Beratan and J. J. Hopfield, J. Am. Chem. Soc. **106**, 1584 (1984).
[8] M. Magoga and C. Joachim, Phys. Rev. B **57**, 1820 (1998).
[9] C. Girard, C. Joachim, and S. Gauthier, Rep. Prog. Phys. **63**, 893 (2000).
[10] V. J. Langlais, R. R. Schlittler, H. Tang, A. Gourdon, C. Joachim, and J. K. Gimzewski, Phys. Rev. Lett. **83**, 2809 (1999).
[11] M. Di Ventra, S. T. Pantelides, and N. D. Lang, Phys. Rev. Lett. **84**, 979 (2000).
[12] L. E. Hall, J. R. Reimers, N. S. Hush, and K. Silverbrook, J. Chem. Phys. **112**, 1510 (2000).
[13] A. A. Demkov, X. Zhang, and D. A. Drabold, Phys. Rev. B **64**, 125306 (2001).
[14] Y.-C. Chang and J. N. Shulman, Phys. Rev. B **25**, 3975 (1982).
[15] W. Franz, *Handbook of Physics* (Springer, Berlin, 1956), Vol. 17, p. 155.
[16] W. Kohn, Phys. Rev. **115**, 809 (1959).
[17] J. B. Krieger, Phys. Rev. **156**, 776 (1967).
[18] J. Bardeen, Phys. Rev. **71**, 717 (1947).
[19] V. Heine, Phys. Rev. **138**, A1689 (1965).
[20] C. Tejedor, F. Flores, and E. Louis, J. Phys. C **10**, 2163 (1977).
[21] J. Tersoff, Phys. Rev. Lett. **52**, 465 (1984).
[22] F. Flores and J. Ortega, Appl. Surf. Sci. **56/58**, 301-310 (1992).
[23] E. H. Rhoderick and R. H. Williams, *Metal-Semiconductor Contacts*, 2nd ed. (Clarendon, Oxford, 1988), Chap. 1.
[24] R. E. Allen, Phys. Rev. B **19**, 917 (1979); **20**, 1454 (1979).
[25] J. J. Rehr and W. Kohn, Phys. Rev. B **9**, 1981 (1974).
[26] O. F. Sankey, R. E. Allen, S. F. Ren, and J. D. Dow, J. Vac. Sci. Technol. B **3**, 1162 (1985).
[27] C. Y. Fong, *Electrons and Phonons in Layered Crystalline Structures* (Reidel, Boston, 1979), p. 59.
[28] D. H. Lee and J. D. Joannopoulos, Phys. Rev. B **23**, 4988 (1981).
[29] J. N. Shulman and Y.-C. Chang, Phys. Rev. B **24**, 4445 (1981).
[30] K. Wood and J. B. Pendry, Phys. Rev. Lett. **31**, 1400 (1973).
[31] J. A. Appelbaum and D. R. Hamann, Phys. Rev. B **6**, 2166 (1972).
[32] R. W. Hardy and R. E. Allen, Surf. Sci. **61**, 177 (1976).
[33] W. H. Press, B. P. Flannery, S. A. Teukolsky, and W. T. Vetterling, *Numerical Recipes: The Art of Scientific Computing* (Cambridge University Press, Cambridge, England, 1989), Chap. 2.
[34] C. D. Bain, E. B. Troughton, Y. T. Tao, J. Evall, G. M. Whitesides, and R. G. Nuzzo, J. Am. Chem. Soc. **111**, 321 (1989).
[35] G. E. Poirier, Chem. Rev. **97**, 1117 (1997).
[36] R. G. Nuzzo, B. R. Zegarski, and L. H. Dubois, J. Am. Chem. Soc. **109**, 733 (1987).
[37] X. D. Cui, X. Zarate, J. K. Tomfohr, O. F. Sankey, A. Primak, A. L. Moore, T. A. Moore, D. Gust, G. Harris, and S. M. Lindsay, Nanotechnology **12**, 1 (2001).
[38] J. P. Lewis, K. R. Glaesemann, G. A. Voth, J. Fritsch, A. A. Demkov, J. Ortega, and Otto F. Sankey, Phys. Rev. B **64**, 195103 (2001); A. A. Demkov, J. Ortega, O. F. Sankey, and M. P. Grumbach, *ibid.* **52**, 1618 (1995); O. F. Sankey and D. J. Niklewski, *ibid.* **40**, 3979 (1989).
[39] The extended orbital calculations have been performed using the SIESTA code written by Pablo Ordejón, Daniel Sánchez-Portal, Emilio Artacho, José M. Soler, and Alberto García: P. Ordejón, E. Artacho, and J. M. Soler, Phys. Rev. B **53**, 10 441 (1996); D. Sánchez-Portal, P. Ordejón, E. Artacho, and J. M. Soler, Int. J. Quantum Chem. **65**, 453 (1997).
[40] D. R. Lide, *CRC Handbook of Chemistry and Physics*, 3rd electronic ed. (CRC Press, Boca Raton, 2001).
[41] Y. Xue, S. Datta, and M. A. Ratner, J. Chem. Phys. **115**, 4292 (2001).
[42] The planewave calculations have been performed using the Vienna *ab initio* Simulation Program (VASP), developed at the Institut für Theoretiche Physik of the Technische Universität Wien: G. Kresse and J. Furthmüller, Comput. Mater. Sci. **6**, 15 (1996); G. Kresse and J. Hafner, Phys. Rev. B **47**, 558 (1993); G. Kresse and J. J. Furthmüller, *ibid.* **54**, 11 169 (1996).